Strain-induced bandgap transition in III-V semiconductors

Badal Mondal[1,2] and Ralf Tonner-Zech[2]

[1]Fachbereich Physik, Philipps-Universität Marburg, 35032 Marburg, Germany
[2]Wilhelm-Ostwald-Institut für Physikalische und Theoretische Chemie, Universität Leipzig, 04103 Leipzig, Germany

After silicon (Si), which revolutionized the world in terms of modern electronics; the discovery of a new family of semiconductors, III-V semiconductors, reshaped the world in terms of modern optoelectronics. Thanks to their unique characteristics of tunable electronic properties their diverse application stretched from our daily household LED to modern LASER, solar cell to optical telecommunication, to modern solar hydrogen production technology are only a few of them to mention. It is already known for quite a long time that different external effects (strain) affect the electronic properties of materials[1,2]. And both from experimental and theoretical perspectives, people are trying to understand how this strain affects the different electronic properties of III-V materials, with the goal of either using them for our good or sometimes to avoid them. One of such electronic properties that makes the so-called backbone of optical properties of III-V semiconductor is bandgap, both in terms of its magnitude and nature. Despite several past attempts the field still remains scientifically alluding to date. In the interest of a deep and thorough understanding in this respect, our goal is to develop a systematic strategy for such analyses using the tool of computational method, modern *ab-initio* density functional theory (DFT); with the advantage of the ability to explore beyond the limitations of simple analytical model approaches.

Despite being a quite successful tool in the fields of molecular chemistry, DFT approaches remained less so in solid-state semiconductors until recently[3,4]. The recent improvement in terms of improved functionals has been proven to gain tremendous success for electronic property analyses of semiconductor materials. Particularly, the exchange-correlation potential functional, TB09 (also known as LDA-mBJ), developed by Tran and Blah[3], which combines the metaGGA exchange potential with LDA correlation, performs at a similar accuracy as the quasiparticle method GW in predicting bandgap of semiconductors and outperforms (range-separated) hybrid functionals in terms of computational efficiency[3,4].

In our first project on binary III-V semiconductors using the TB09 functional implemented in the Vienna *ab-initio* simulation package (VASP-5.4.4) we have shown that depending on the way as well as the strength of the applied strain, the material behavior can change substantially, namely, a direct bandgap semiconductor can transform to an indirect bandgap semiconductor or vice versa. We have shown the transition of well-known direct bandgap semiconductor GaAs to indirect bandgap at about 1.56 % isotropic compressive strain which however goes to the 3.52 % tensile strain when biaxial strain is considered (Fig. 1).

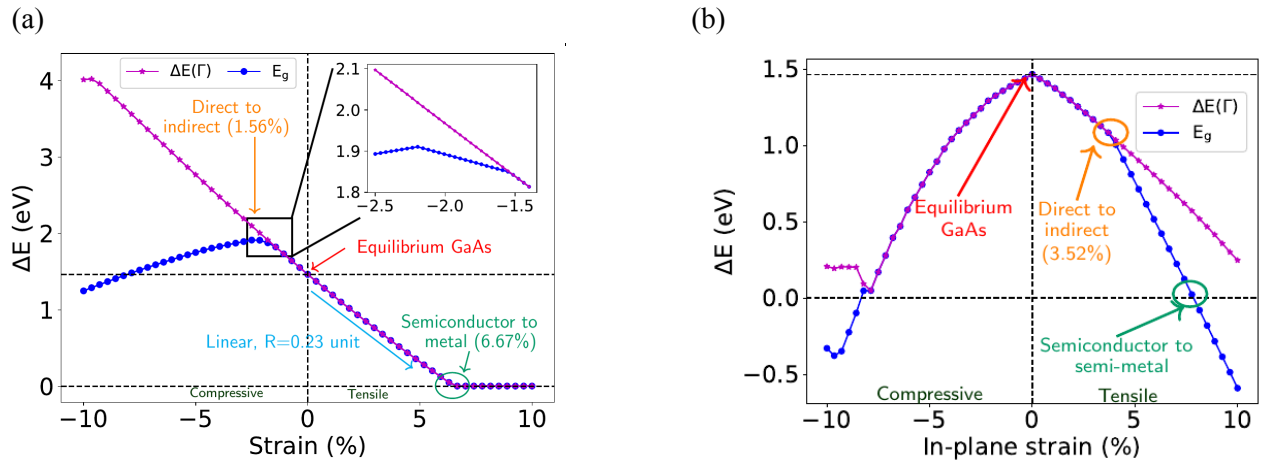

Figure 1: Variation of the energy difference between the conduction band and valence band at the Γ point (ΔE(Γ)), and the energy difference between conduction band minima and valence band maxima (E_g) for GaAs under (a) isotropic strain and (b) biaxial strain.

Mar 15, 2022

Alongside the direct-indirect transition, we are also able to pinpoint the whole transition path over quite a large strain region (± 10 %). Using the orbital analysis we have shown the difference in the 's' and 'p'-orbital character resulted in the strong wave vector dependency of the band energies, which ultimately led to the transitions under different strains. Following the same principle, the transitions in other commonly used binary III-V semiconductors (including Si) are also analyzed as tabulated in Table 1.

Table 1: Different transitions in the nature of bandgap for binary III-V semiconductors

System	Transition**			Conduction band minima transition path	
	Type*	Isotropic strain(%)	Biaxial strain(%)	Isotropic strain	Biaxial strain
Si	IDT	10.31 (t)	×	$\Delta_m \rightarrow L \rightarrow \Gamma$ (t)	$\Delta_m \rightarrow K \rightarrow L$ (c)
GaP	IDT	2.63 (t)	×	$\Delta_m \rightarrow L \rightarrow \Gamma$ (t)	$\Delta_m \rightarrow L$ (c)
GaAs	DIT	1.56 (c)	3.52 (t)	$\Gamma \rightarrow L \rightarrow \Delta_m \rightarrow X$ (c)	$\Gamma \rightarrow \Delta_m$ (t)
GaSb	DIT	1.00 (c)	3.71 (t)	$\Gamma \rightarrow L \rightarrow \Delta_m$ (c)	$\Gamma \rightarrow \Delta_m$ (t)
InP	DIT	4.40 (c)	7.66 (t)	$\Gamma \rightarrow X$ (c)	$\Gamma \rightarrow \Delta_m$ (t)
InAs	DIT	7.41 (c)	×	$\Gamma \rightarrow X$ (c)	×
InSb	DIT	5.18 (c)	×	$\Gamma \rightarrow L \rightarrow \Delta_m$ (c)	×

* DIT and IDT correspond to the direct to indirect and indirect to direct transition, respectively.
** The 't' and 'c' in brackets correspond to the compressive and tensile strain, respectively.
× No transitions within ± 10 % of the strain.
Δ_m ≡ k-point coordinate of [0.0000, 0.4282, 0.4282] in reciprocal space.

Following the great success in binary systems, our next goal was to extend the analyses for higher-order systems. However, in comparison to the binary systems where we could use simple primitive cells for the analysis but in multinary systems, to ensure the ideal admixing among all the components in the composition we had to go for supercell[5]. Unfortunately, the use of this supercell resulted in the well-known 'band folding'[6,7] phenomena. Due to this band folding, although it was straightforward to get the information about the magnitude of bandgap, but not the nature of bandgap, which however is the most essential component for the analysis of direct-indirect transition. Alongside this would tremendously increase the computational cost as well. So, in our next project, we aimed for developing a relatively cost-effective systematic approach for bandgap transition analysis in the next higher-order ternary systems. Using the idea of 'Bloch spectral density/weight'[8,9] we have developed a systematic strategy for the direct-indirect transition analysis in the ternary systems ultimately enabling us to construct the 'bandgap phase diagram'[10] by mapping the different direct-indirect transition points with composition and strain, as is shown in Fig. 2. Extrapolating our analyses from binary systems we also have shown the relative band energy differences only in the conduction band at the Γ, L, and (near) X point in the band structure of zincblende structure as the primary source of alteration in the nature of bandgap. Based on this observation, then by appropriately choosing the supercell size and hence, by pre-controlling the folding pattern we have shown the excellent effectiveness of our algorithm in keeping the computational cost at its minimum with the minimum loss of most important information that we were needed for the analyses. In combination with the compositional (thermodynamic) phase diagram, we have shown that the bandgap phase diagram, this new way of mapping the effect of strain in III-V ternary (and higher-order material) can significantly improve the future development in terms of strategic choice of certain application-oriented most suited material systems or vice versa.

Following the footstep of our previous analyses, we then extended the scope to the next higher order quaternary systems. However, given the huge compositional space, it will be an extremely daunting step to

take to cover enough of the vast compositional space in quaternary systems using DFT calculations only.

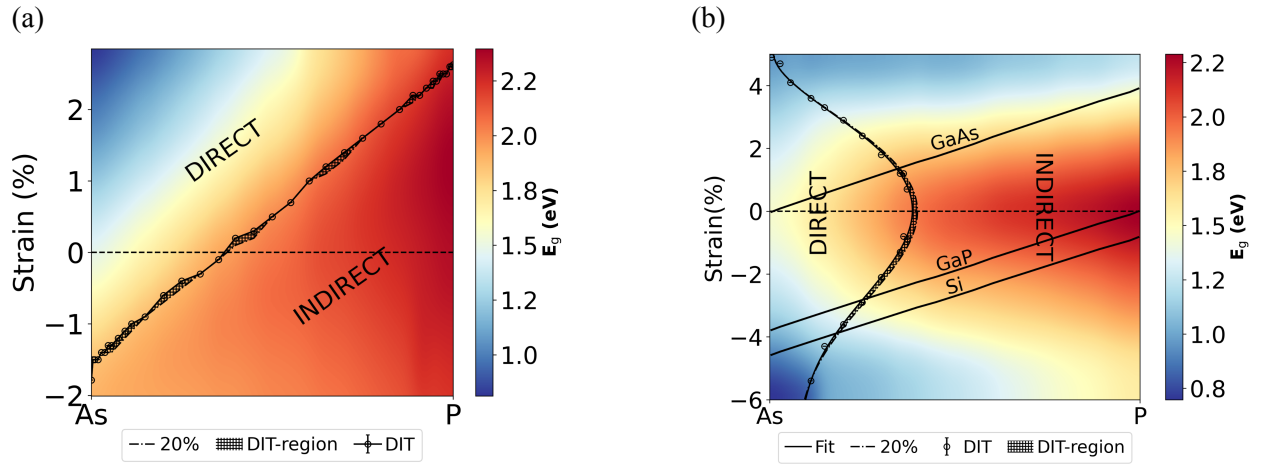

Figure 2: GaAsP bandgap phase diagram under (a) isotropic strain and (b) biaxial strain. The color scale in the figures corresponds to the bandgap magnitude (E_g). The DIT points at each composition are averaged over 10 random configurations. 20 % uncertainty curve corresponds to the shift in the DIT points when a cutoff of 20 % Bloch weight is chosen as the minimum requirement for a (defect) state to be considered as a defined state. The positive and negative strain corresponds to the tensile and compressive strain respectively. In figure-b, the DIT points are fitted with 5th order polynomial. The GaAs, GaP, and Si lines correspond to the substrate strain line under the 'epitaxial growth' model.

So, we decided to take the advantage of another uprising modern scientific tool Machine learning. The core idea is to combine our limited DFT capability with the easily extendable ML with the hope to cover the maximum compositional space with reliable results. We started with the quaternary compound GaAsPSb. Using the already available DFT data for the corresponding ternary subsystems of our quaternary system of choice and some more calculations on the quaternary region we have mapped the DIT points over composition and scanned over strain; Fig. 3 and 4. Here, we have used the Support Vector Machine (SVM) supervised machine learning model in combination with Radial Basis Function (RBF) kernel. For the prediction of bandgap nature, we used the classification version of the SVM model, known as the Support Vector Classification (SVC) model with an accuracy of 95.4%. And the regression version of SVM, the Support Vector Regression (SVR) model for the prediction of the bandgap with an accuracy (r2 score) of 99%.

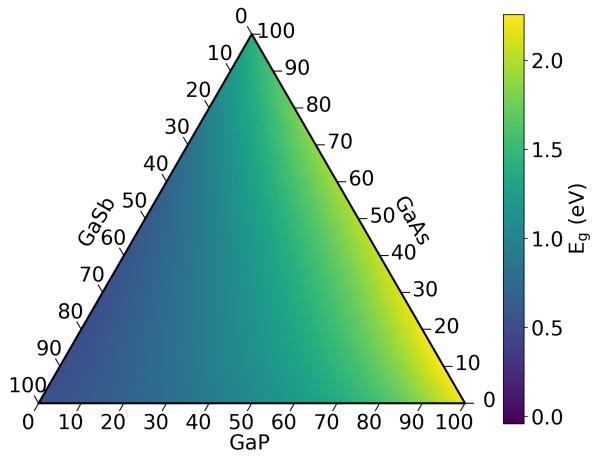

Figure 3: Mapping of bandgap magnitude (E_g) over the whole composition space of GaAsPSb at equilibrium configurations (strain=0%).

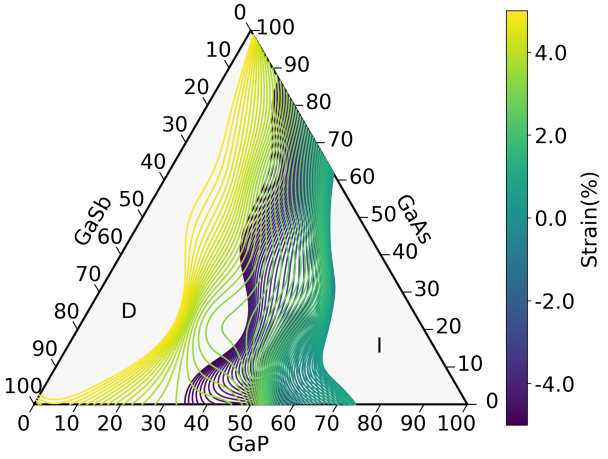

Figure 4: Mapping of DIT lines within ≤ ±5% of strain. The 'D' and 'I' symbolize the 'Direct' and 'Indirect' bandgap region, respectively.

Mar 15, 2022

Alongside electronic properties, the realization of efficient and stable optoelectronics requires the smooth transportation of electrons through the system. The presence of any kind of dislocation, heterogeneity in the material composition, or roughness in the heterostructure interfaces can tremendously hinder the electronic mobility and hence, the performance and long-term stability of the devices. So, with the goal of understanding the morphological stability of the system, in another parallel project, we aimed to map the different regions of stability considering the combined effect of thermodynamic phase separation[11,12,13] and kinetic instabilities (critical thickness)[14,15,16]. As a system of choice, we used a well-known nitride system, GaAsPN. Using simple mean-field ansatz, we have shown that GaAsPN grown on GaP or Si as the substrate is a thermodynamically stable compound over the entire composition range at and above room temperature. Through kinetic analysis, critical compressive mismatch strains have been predicted, beyond which the epitaxy layer undergoes strain-induced instability, forming roughness on a perfectly flat surface or introducing dislocation (Fig. 5). We have shown the lattice-mismatch-driven transition in the instability mechanism from misfit dislocation to Stranski-Krastanov (SK) type surface roughness. In the region of relatively small lattice mismatch (less than 1 % mismatch in GaAsPN); the main source of instability is the misfit dislocation whereas for comparatively high lattice mismatch (greater than 1 % mismatch) the dominant determinant of surface morphology is the SK-type transition. Although experimentally[17,18,19,20] due to limitations in accurate determination of critical thickness, the quantitative matching in terms of critical thicknesses are not possible, but the observed instability mechanisms at different GaAsPN composition qualitatively match quite nicely with our theoretical results (Fig. 5). We have shown that in GaAsPN whereas the lattice mismatch strain (and also the high elastic coefficient of GaN) decreases the thermodynamic instability but it increases the kinetic instability, such that the combination thereof determines the overall stability. As the generalization of this concept, by combining thermodynamics with kinetics we have developed a strategy to optimize the best substrate-layer pair in heteroepitaxy. We have shown the best suitable substrate for the epitaxial growth of GaAsPN at around 800 K temperature with a reasonable thickness over a good range of composition with nitrogen percentage of as much as ~ 40 – 50 % is the substrate with lattice constant (a_s) ~ 5.1 Å. Above this a_s the N-solubility is restricted by the kinetic instability and below this a_s thermodynamic instability starts to dominate. Replacing gallium with indium, in InAsPN, the increase in mismatch strain pushed the thermodynamic instability towards dominance as expected (Fig. 6). Note that, although these mean-field models are proved to be best in giving the global picture with quite a good accuracy, for quantitative precision, however, one should aim for improved much more accurate models such as (kinetic) Monte Carlo, quantum chemical modeling.

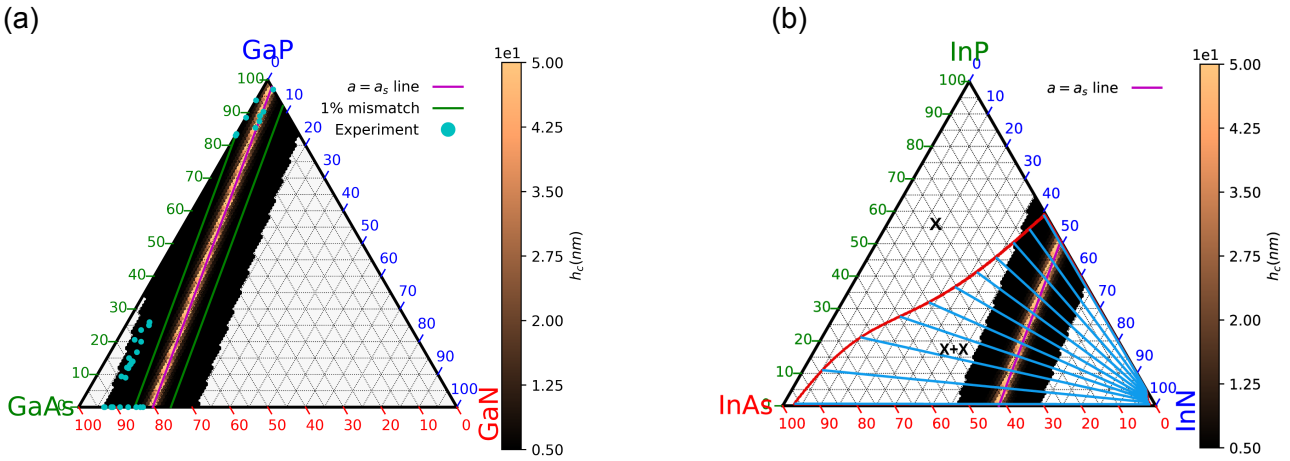

Figure 5: Thermodynamic phase diagram combined with the kinetic critical thicknesses (h_c) for (a) GaAsPN and (b) InAsPN grown on Si substrate at 800K. The $a = a_s$ line is the substrate-layer lattice-matched line. 'x' and 'x+x' correspond to the single and binodal phase separation regions, respectively. The cyan lines are the tie lines in the binodal phase separation region.

Acknowledgments
We would like to thank HRZ Marburg, GOETHE-CSC Frankfurt, ZIH TU Dresden, and HLR Stuttgart for providing the computational resources.

References
[1] T. B. Boykin, G. Klimeck, R. C. Bowen, R. Lake, Phys. Rev. B 1997, 56, 4102
[2] Y. Sun, S. E. Thompson, T. Nishida, J. Appl. Phys. 2007, 101, 104503
[3] F. Tran, P. Blaha, Phys. Rev. Lett. 2009, 102, 226401
[4] P. Rosenow, L. C. Bannow, E. W. Fischer et al., Phys. Rev. B 2018, 97, 075201
[5] P. R. C. Kent, A. Zunger, Phys. Rev. B 2001, 64, 115208
[6] W. Ku, T. Berlijn, C.-C. Lee, Phys. Rev. Lett. 2010, 104, 216401
[7] S.-Y. Yang, H. Yang, E. Derunova et al., Adv. Phys.: X 2018, 3, 1414631
[8] V. Popescu, A. Zunger, Phys. Rev. Lett. 2010, 104, 1
[9] O. Rubel, A. Bokhanchuk, S. J. Ahmed, E. Assmann, Phys. Rev. B 2014, 90, 115202
[10] https://bmondal94.github.io/Bandgap-Phase-Diagram/
[11] G. B. Stringfellow, J. Cryst. Growth 1974**,** 27, 21
[12] J. W. Cahn, Acta Metallurgica 1961, 9, 795
[13] G. B. Stringfellow, J. Cryst. Growth 1983, 65, 454
[14] G. Dubrovskii, E. Cirlin, M. Ustinov, Phys. Rev. B 2003, 68, 1
[15] D. V. Yurasov, Yu. N. Drozdov, Semiconductors 2008, 42, 563
[16] J. W. Matthews, A. E. Blakeslee, J. Cryst. Growth 1974, 27, 118
[17] T. Wegele, A. Beyer, P. Ludewig et al., J. Phys. D: Appl. Phys. 2016, 49, 075108
[18] P. Ludewig, S. Reinhard, K. Jandieri et al., J. Cryst. Growth 2016, 438, 63
[19] P. Ludewig, M. Diederich, K. Jandieri, W. Stolz, J. Cryst. Growth 2017, 467, 61
[20] T. Wegele, A. Beyer, S. Gies et al., J. Appl. Phys. 2016, 119, 025705